



# Synthesis, structural and magnetic properties of self-organized single-crystalline nanobricks of chalcopyrite $\text{CuFeS}_2$

Igor S. Lyubutin<sup>a,\*</sup>, Chun-Rong Lin<sup>b,\*,1</sup>, Sergey S. Starchikov<sup>a</sup>, Yu-Jhan Siao<sup>b</sup>,  
Muhammad Omar Shaikh<sup>b</sup>, Konstantin O. Funtov<sup>a</sup>, Sheng-Chang Wang<sup>b</sup>

<sup>a</sup> Shubnikov Institute of Crystallography, Russian Academy of Sciences, Moscow 119333, Russia

<sup>b</sup> Institute of Nanotechnology and Department of Mechanical Engineering, Southern Taiwan University of Science and Technology, Tainan 71005, Taiwan

Received 23 October 2012; received in revised form 4 March 2013; accepted 12 March 2013

## Abstract

A thermal pyrolysis method has been developed to synthesize the tetragonal phase of chalcopyrite magnetic semiconductor  $\text{CuFeS}_2$  nanoparticles. All nanoparticles have the same anisotropic brick-like shape, and the “bricks” are self-organized in a certain orientation, creating well-ordered nanocomposites. High-resolution transmission electron microscopy and electron diffraction data show that every nanobrick is a single crystal with a layered atomic structure and characteristic dimensions of about  $5 \text{ nm} \times 20 \text{ nm}$  in plane. Magnetic measurements support the antiferromagnetic spin structure and reveal the appearance of a small ferromagnetic component below 60 K. Magnetic anomalies observed in the zero-field cooled magnetization curves at low temperatures may be related to an appearance of magnetic moment at the Cu ion site. The Mössbauer spectra show that only about 50% of Fe atoms are in the magnetically ordered  $\alpha$ -phase of chalcopyrite. The remaining Fe is non-magnetic and may be located either in the  $\gamma$ -phase of chalcopyrite or in isocubanite. Crown Copyright © 2013 Published by Elsevier Ltd. on behalf of Acta Materialia Inc. All rights reserved.

**Keywords:** Self-organized single crystal; Magnetic properties; Mössbauer spectroscopy

## 1. Introduction

Ternary chalcogenide compounds have recently attracted great attention due to their important physical and chemical properties and promising potential applications in solar power engineering and spintronics [1–12]. Chalcopyrites compounds such as  $\text{CuAlS}_2$ ,  $\text{CuInSe}_2$ ,  $\text{CuGaSe}_2$ ,  $\text{CuInS}_2$  and  $\text{CuFeS}_2$  are typical representatives of the ternary chalcogenide family. They are semiconductors with a very broad band gap distribution from 3.5 to 0.6 eV [13]. They have been intensively studied and polycrystalline thin films of some of these compounds are utilized in solar cells [14]. Utilizing the semiconductor nanocomposites in solar cells can

reduce their cost and improve their efficiency to the value for bulk materials. An efficiency of 18.2% for solar cells made of nanostructured silicon has been reported, which is close to the value of commercially available crystalline silicon devices [15]. Nanocrystals of chalcopyrite  $\text{CuFeS}_2$  have recently attracted the attention of scientists. Thin films [16], nanowires [17], nanorods and spherical particles [18] and nanocrystals [19–21] have been synthesized to investigate the properties of this compound in view of possible applications in photovoltaics, thermoelectric and spintronic devices. It was found that nanoparticles have a larger band gap (1.2 eV) than that of bulk chalcopyrite (0.6 eV) and this feature depends on size [21]. Comparing the thermoelectric properties of nanosized chalcopyrite with those of bulk material, a significant increase in the power factor and a tremendous reduction of thermal conductivity has been observed, thus enhancing the efficiency of thermoelectric materials (figure of merit) by 77 times [21].

\* Corresponding authors. Tel.: +7 499 135 6250; fax: +7 499 135 1011.

E-mail addresses: [lyubutin@ns.crys.ras.ru](mailto:lyubutin@ns.crys.ras.ru) (I.S. Lyubutin), [erlin@mail.stut.edu.tw](mailto:erlin@mail.stut.edu.tw) (C.-R. Lin).

<sup>1</sup> Tel.: +886 6 2533131x3547; fax: +886 6 2425092.

Special attention has been focused on the development of new methods for preparing nanocrystalline composites which are expected to have important properties as building blocks for many novel functional materials [17,22–24]. Different approaches to the growth of nanostructured Cu-containing chalcogenides have been reported [25], many of them based on solvothermal reactions leading to the formation of powders. Nanocrystals of the semiconducting chalcopyrite  $\text{CuFeS}_2$  have been synthesized, utilizing a facile solution-based method [20]. Depending on the choice of precursors and synthesis conditions, the nanocrystals exhibit either a spherical (12 nm) or pyramidal morphology (30 nm). The larger size pyramidal nanoparticles exhibit a band gap (0.52 eV) close to the bulk, whereas a larger band gap (0.95 eV) was obtained for the smaller spherical particles. Because of the very broad absorption characteristics and tunable band gap, the  $\text{CuFeS}_2$  nanoparticles are potentially useful for the fabrication of solar cells.

Bulk  $\text{CuFeS}_2$  compound is a magnetic semiconductor with a chalcopyrite structure [26–30]. It has a very small optical energy gap (0.5–0.6 eV) [30] and a very high Néel temperature ( $T_N = 823$  K) [26–28]. The crystal lattice of  $\text{CuFeS}_2$  is tetragonal with parameters  $a = 5.29$  Å and  $c = 10.41$  Å, and space group  $I\bar{4}2d$  [31]. Metallic atoms Cu and Fe have almost perfect tetrahedral coordination with four neighboring sulfur ions. Alternating metal Fe and Cu layers are separated by the sulfur layers. It is known that at least two ionic states,  $\text{Cu}^{1+}\text{Fe}^{3+}(\text{S}^{2-})_2$  and  $\text{Cu}^{2+}\text{Fe}^{2+}(\text{S}^{2-})_2$  are possible in chalcopyrite [31,32]. However the relationship between the ionic states and the magnetic and electric properties of  $\text{CuFeS}_2$  is not clearly understood.

In the present paper, a thermal pyrolysis route was developed to synthesize chalcopyrite nanoparticles. X-ray diffraction (XRD), high-resolution transmission electron microscopy (HRTEM), electron diffraction, magnetic and Mössbauer spectroscopy measurements were used for characterization of the obtained nanocomposites.

## 2. Sample preparation and characterization techniques

In a typical process for  $\text{CuFeS}_2$  nanocomposite preparation, 1 mmol of copper acetate monohydrate ( $\text{Cu}(\text{COOCH}_3)_2 \cdot \text{H}_2\text{O}$ ), 1 mmol of iron acetate ( $\text{Fe}(\text{COOCH}_3)_2$ ), 3 mmol of sulfur powder, and 10 g of octadecylamine (ODA) were put into a three-necked flask equipped with an inlet of argon gas, condenser, magnetic stirrer, thermocouple and heating mantle. The mixture was heated up to

100 °C after which 1 ml of trioctylphosphine (TOP) was added into the mixture. After 10 min of magnetic stirring, the system was heated further to 240 °C (or 320 °C) and maintained at this temperature for 1 h for nanoparticle growth and crystallization. The reaction temperature was adjusted to obtain size-controlled  $\text{CuFeS}_2$  nanocomposites. After the reaction the resulting  $\text{CuFeS}_2$  nanocomposites were collected via centrifugation and rinsed with a solvent (composed of toluene and methanol) at 70 °C several times to remove the ODA. Then the compound was dried in a vacuum at 70 °C for 6 h. The reaction conditions are shown in Table 1.

The crystal structure and phase purity of the samples were examined by powder XRD (Mutiflex MF2100, Rigaku Co. Ltd.). The morphology and microstructure of the particles were characterized by HRTEM (Tecnai G2 F20, FEI-TEM, Philips Co. Ltd.) and electron diffraction. Magnetic measurements were performed using a superconducting quantum interference device (SQUID-VSM, MPMS, Quantum Design) in applied fields up to 7 T. For measurements of the zero-field-cooled (ZFC) and field-cooled (FC) temperature dependence of magnetization, the samples were first cooled at zero field from 300 to 5 K and then the magnetization was measured in a field of 50 Oe by heating the sample from 5 to 300 K. After that the samples were cooled from 300 to 5 K maintaining the same field. Then the FC curves were recorded with increasing temperature.

Mössbauer spectroscopy was applied to examine the phase composition, structural and magnetic properties of the nanoparticles. The  $^{57}\text{Fe}$ -Mössbauer spectra were recorded at room temperature in transmission geometry with a standard spectrometer operating in the constant acceleration regimes. The gamma-ray source  $^{57}\text{Co}(\text{Rh})$  was at room temperature and the isomer shifts were measured relative to metal iron ( $\alpha\text{-Fe}$ ).

## 3. Results and discussion

### 3.1. XRD and electron microscopy data

The crystal structure and phase purity of the samples were examined using powder XRD. As shown in Fig. 1, all reflections can be readily indexed to the tetragonal phase of chalcopyrite  $\text{CuFeS}_2$ . We found that the  $\text{CuFeS}_2$  particle size could be controlled via the relative concentration of the iron and sulfur sources, the reaction time and reaction temperatures. Details of the process for the selected samples are described and summarized in Table 1.

Table 1  
Some details of the synthesis of the  $\text{CuFeS}_2$  nanocomposites.

Sample name	Composition	Reaction scheme	Crystal structure	$d$ (nm)
CFS112A	$\text{CuFeS}_2$	$\text{C} + \text{F} + \text{S} + \text{ODA} \rightarrow 100$ °C, +TOP, 10 min $\rightarrow$ 240 °C, 1 h	Tetragonal	4.7
CFS112B	$\text{CuFeS}_2$	$\text{C} + \text{F} + \text{S} + \text{ODA} \rightarrow 100$ °C, +TOP, 10 min $\rightarrow$ 320 °C, 1 h	Tetragonal	37

C =  $\text{Cu}(\text{COOCH}_3)_2 \cdot \text{H}_2\text{O}$ , F =  $\text{Fe}(\text{CH}_3\text{COO})_2$ , S = sulfur powders, ODA = octadecylamine, TOP = trioctylphosphine, and  $d$  is the average size of the nanoparticles obtained from the XRD data.

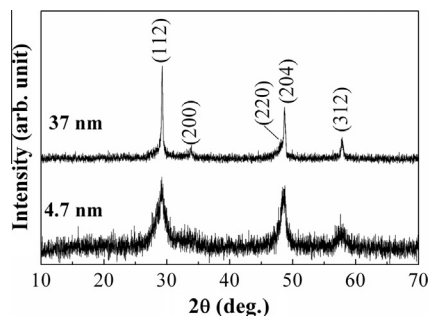


Fig. 1. XRD patterns of  $\text{CuFeS}_2$  nanoparticles with crystallite size 4.7 and 37 nm. All reflections can be indexed to the chalcopyrite phase  $\text{CuFeS}_2$  with tetragonal cell.

An estimation of the crystallite size by Scherrer's formula of peak broadening [33] gives for two samples average crystallite sizes of 4.7 and 37 nm.

The particle shape and size were examined by HRTEM. The HRTEM images (Fig. 2a,b) show that all nanoparticles have the same anisotropic shape of "bricks" which are self-organized in a certain orientation, creating well-ordered nanocomposites. The characteristic length of nanobricks is about 20–25 nm and their height is about 5–6 nm. Every brick particle is separated from its neighbors by intercalations which are supposed to be the

octadecylamine surfactant (Fig. 2b). The distance between the brick particles is about 3–3.5 nm.

It should be noted that the particle size can differ substantially from the sizes of the crystallites, which may be due to the presence of amorphous layers between the crystallites and/or by aggregation of the crystallites. We found that the size of single nanobricks is nearly the same in the particles prepared at different conditions but the character of the brick's aggregation is different. Fig. 2b clearly shows that each nanobrick is a single crystal with a layered atomic structure. The layered structure is shown by the black and white stripes oriented along the length of the brick. Each black and white stripe is about 3 Å wide (see insert in Fig. 2b). The electron diffraction pattern (Fig. 2c) supports the crystalline nature of the nanobricks and indicates the body-centered tetragonal lattice of chalcopyrite  $\text{CuFeS}_2$ . The calculated interplanar distances are 3.08 Å (112), 1.90 Å (220) and 1.87 Å (204). It is established that the nanobricks are self-packed normal to the (112) plane with the long axis of bricks in this plane. As is shown in the enlarged section of Fig. 2b, the lattice spacing of 3.08 Å between two adjacent lattice planes corresponds to that of (112) crystal planes in  $\text{CuFeS}_2$ .

The nearly monodisperse  $\text{CuFeS}_2$  nanobricks were synthesized by rapid pyrolysis of raw materials

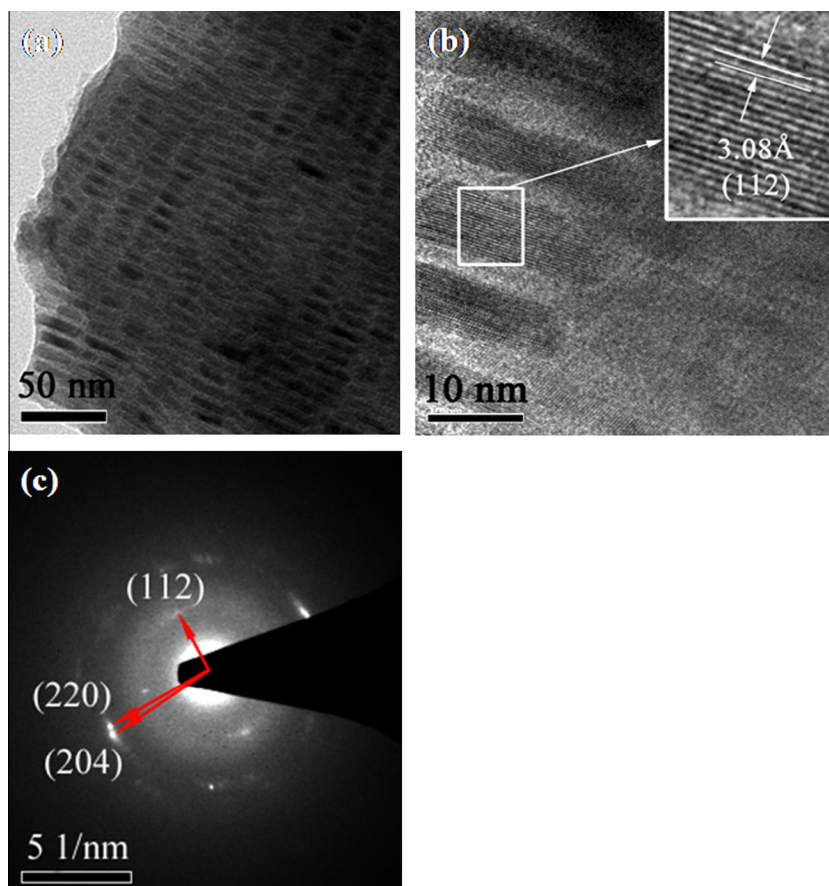


Fig. 2. The high-resolution transmission electron microscopy images (a and b) and the electron diffraction pattern (c) of the  $\text{CuFeS}_2$  nanoparticles (4.7 nm sample) showing the self-organized nanobricks. The single-crystal structure can be seen in HRTEM images with enlarged scale (b).

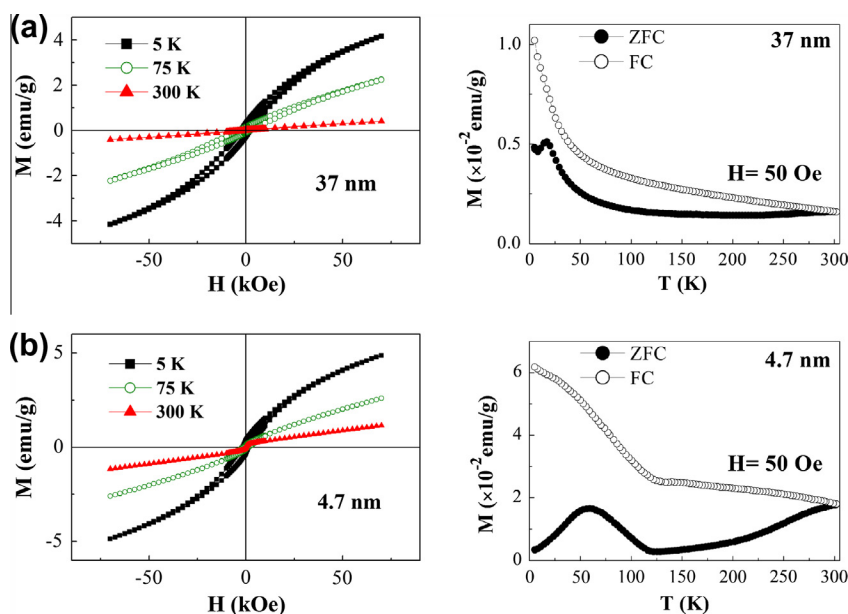


Fig. 3. The applied field dependences of magnetization and hysteresis loops at different temperatures (a) and temperature dependences of the ZFC and FC magnetization (b), recorded in an applied magnetic field of 50 Oe, for the CuFeS<sub>2</sub> nanoparticles 37 and 4.7 nm in size.

(Cu(COOCH<sub>3</sub>)<sub>2</sub>·H<sub>2</sub>O, Fe(COOCH<sub>3</sub>)<sub>2</sub> and sulfur powder) in the presence of a surfactant mixture composed of ODA and TOP. The effect of the ODA surfactant is noticeable in many ways: (i) it is responsible for their uniform anisotropic growth into bricks; (ii) it stabilizes the nanobricks; and (iii) it defines the lateral spacing between the nanobricks. TEM images (Fig. 2a and b) reveal the formation of aligned CuFeS<sub>2</sub> nanobrick arrays via the face-to-face and edge-to-edge formation when the nanobricks are capped by ODA ligands.

In a colloidal system, attractive forces between nanocrystals, such as van der Waals and dipole–dipole interactions, may influence the structural organization behavior of the system. The dipole–dipole interaction is a ubiquitous driving force available for self-assembly, particularly in the case of nanocrystals with non-spherical symmetry, i.e. the surfaces are not covered by the same crystallographic facets [34]. The polarity difference between crystallographic facets on nanocrystals may create a dipole within the nanocrystals. Moreover, different crystallographic facets should display a different affinity for coupling with different functional ligands. Thus, the ligand population on nanocrystal surfaces can be expected to be anisotropic rather than isotropic. In our case, the anisotropic capping on nanobricks can be used to enhance the dipole–dipole interactions between nanobricks for the orientational “self-organization”.

### 3.2. Magnetic measurements

Magnetization curves  $M(H)$  of the 4.7 and 37 nm size samples reveal antiferromagnetic behavior at temperatures between 70 and 300 K (Fig. 3a). At fixed magnetic fields, the magnetization increases with lowering temperature,

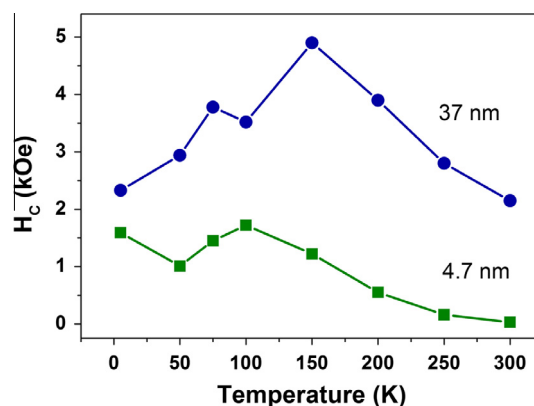


Fig. 4. Temperature dependences of coercive field  $H_c$  for the 4.7 and 37 nm size nanoparticles.

especially in the case of the 4.7 nm size sample (Fig. 3a). This is consistent with the more disordered state of the 4.7 nm size sample, as follows from the XRD data. At 50 and 5 K hysteresis is observed in the  $M(H)$  curves of both samples, indicating the appearance of a small ferromagnetic component. The coercivity is larger in the 37 nm size sample, indicating the higher magnetic crystalline anisotropy of well-elongated nanobricks. Fig. 4 shows the temperature dependence of coercive field  $H_c$  for the 4.7 and 37 nm size nanoparticles. At low temperature, 5 K, the  $H_c$  value is 1.6 and 2.3 kOe for the 4.7 and 37 nm size particles, respectively. With increasing temperature, the  $H_c$  (4.7 nm) value decreases and reaches almost zero at room temperature. Meanwhile, the  $H_c$  (37 nm) value first increases, showing a maximum of 4.9 kOe at about 160 K, and then decreases to 2.1 kOe at room temperature (Fig. 4). The temperature behavior of  $H_c$  (4.7 nm) is also

not uniform, and shows a maximum at 100 K that is less pronounced than the  $H_c$  (37 nm) maximum.

The temperature dependences of the FC and ZFC magnetizations are shown in Fig. 3b. The ZFC and FC curves measured in the low field of  $H_{\text{ext}} = 50$  Oe are split below  $T_{\text{int}} \approx 300$  K, implying an appearance of magnetic interactions between nanoparticles [35]. The ZFC curve of the 37 nm sample displays a maximum at  $T_B \approx 20$  K. In the 4.7 nm sample, the ZFC magnetization behavior is more complicated. As temperature is lowered from 300 K, the magnetization decreases down to nearly zero at 120 K, then it increases, reaching a maximum at about 60 K, and goes down again to a zero value at the lowest temperature of 5 K. The FC curve also has an anomalous bend near 120 K (Fig. 3b).

As illustrated in the TEM images, the nanobricks are well separated from each other by nonmagnetic intercalated compound (ODA). The maximum in the ZFC curves observed at blocking temperature  $T_B \approx 20$  and  $T_B \approx 60$  K for the 37 and 4.7 nm samples, respectively, may be related to the superparamagnetic properties of the  $\text{CuFeS}_2$  nanoparticles. This behavior is typical for systems of magnetic moments which undergo a spin blocking (or frozen) effect. Above  $T_B$ , particles are in a superparamagnetic state, whereas below  $T_B$ , thermal fluctuations of magnetic moments are blocked by magnetic anisotropy. As we show below, Mössbauer spectra indicate superparamagnetic behavior of small particles, and some fraction of superparamagnetic state is observed in all samples synthesized, which may be caused by the particle separation and also by size distribution.

On the other hand, anomalous behavior in the temperature dependence of the magnetic susceptibility  $\chi(T)$  has been found in the bulk chalcopyrite  $\text{CuFeS}_2$  at temperatures between 60 and 90 K [12]. It is explained by the magnetic phase transition caused by spin ordering of Cu atoms from the paramagnetic to the antiferromagnetic state. A remarkable increase in susceptibility  $\chi(T)$  and magnetization  $M(T)$ , and anomalous heat capacity, has been recently found in bulk  $\text{CuFeS}_2$  at  $T < 100$  K [36]. It is explained by the presence of non-interacting ferromagnetic clusters appearing due to disordering of Fe and Cu atoms in the metal sublattice of chalcopyrite, leading to phase inhomogeneity of the crystal lattice.

### 3.3. Mössbauer spectroscopy data

At room temperature the  $^{57}\text{Fe}$ -Mössbauer spectra of  $\text{CuFeS}_2$  nanoparticles consists of a six-line magnetic hyperfine component and a central doublet non-magnetic component (Fig. 5a and b). This indicates that some of the Fe ions are in the magnetically ordered state (about 45% of total Fe in both the 4.7 and 37 nm size samples), and the other part is in the paramagnetic state (about 55%). A similar non-magnetic component was observed in  $\text{CuFeS}_2$  nanorods synthesized by a hydrothermal reaction

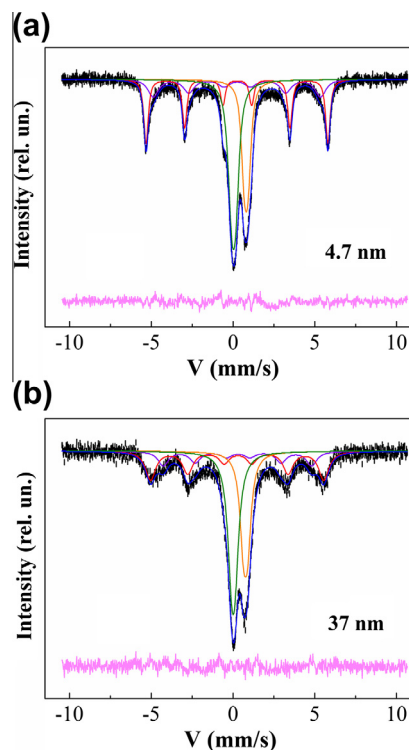


Fig. 5. The room temperature  $^{57}\text{Fe}$ -Mössbauer spectra of the 4.7 nm (a) and 37 nm (b) chalcopyrite  $\text{CuFeS}_2$  nanoparticles. The spectra fitting to magnetic and nonmagnetic components attributed to nonequivalent iron sites are shown by solid lines.

[37], and was explained by presence of an amorphous phase in the product.

The resonance lines of the magnetic component in the 4.7 nm sample have slight asymmetry with broadening in the inner side of lines (Fig. 5a). The magnetic spectra can be made to fit to two components with the magnetic hyperfine fields  $H_{\text{hf}} = 34.54$  (28%) and  $31.54$  (17%) T. The isomer shift  $\delta$  of both magnetic components is almost the same  $\delta = (0.23\text{--}0.24)$   $\text{mm s}^{-1}$  and the quadrupole shifts  $\epsilon$  are near zero. The hyperfine parameters of the magnetic component with  $H_{\text{hf}} = 34.54$  T completely coincide with the parameters for the bulk [38–41] and nanorod chalcopyrite [17,37].

In the 37 nm sample the line broadening of the magnetic component is much higher than in the 4.7 nm sample (Fig. 5b), and the value of magnetic fields  $H_{\text{hf}}$  is spread from 33 to 28 T while  $\delta \approx 0.28$   $\text{mm s}^{-1}$  and  $\epsilon \approx 0.04$   $\text{mm s}^{-1}$ . The line broadening and some distribution of the  $H_{\text{hf}}$  values can be connected with a particle size distribution, and with the superparamagnetic behavior of small particles. An absence of quadrupole splitting shows zero electric field gradient at Fe sites in chalcopyrite, thus suggesting a highly symmetric surrounding of Fe atoms by  $\text{S}^{2-}$  ions.

The relatively low isomer shift  $\delta$  and magnetic field  $H_{\text{hf}}$  values of the magnetic Mössbauer components in our nanoparticles are characteristic of high-spin ferric  $\text{Fe}^{3+}$  ions in the tetrahedral sites of chalcopyrite with strong Fe–S covalency. The isomer shift value for chalcopyrite

nanoparticles is smaller than the  $\delta$  value for high-spin  $\text{Fe}^{3+}$  ions in oxides. This implies a partial delocalization of  $3d$  electrons in the semiconducting compound  $\text{CuFeS}_2$ . In general, the isomer shift in iron sulfides is less than in oxides (both for  $\text{Fe}^{2+}$  and  $\text{Fe}^{3+}$  ions) due to the stronger covalence of the Fe–S bonds as compared with the Fe–O bonds [42,43]. A decrease in  $\delta$  indicates an increase in the  $s$ -electron density at the Fe nuclei. This is explained by delocalization of  $3d$  electrons, which are involved in bonding and hence less effectively shield the nucleus from the  $4s$  electrons [43,44]. It seems that  $3d$  electrons of Cu can also be partly delocalized. A strong p–d hybridization between S and metal ions (both Fe and Cu) was revealed by X-ray absorption near edge structure measurements [45]. This indicates that an intermediate state between the  $\text{Cu}^{1+}\text{Fe}^{3+}\text{S}_2^{2-}$  and  $\text{Cu}^{2+}\text{Fe}^{2+}\text{S}_2^{2-}$  electronic configuration of  $\text{CuFeS}_2$  may be realized [32,46], which leads to appearance of a magnetic moment at the Cu ions [12]. Such an effect can explain the anomalies of magnetization observed in our magnetic measurements at low temperatures. This is also consistent with small values of the magnetic field  $H_{\text{hf}}$  and isomer shift  $\delta$  obtained from the Mössbauer data.

The paramagnetic part of the Mössbauer spectra can be fit to two quadrupole doublets with close values of quadrupole splitting  $\varepsilon \approx 0.20\text{--}0.25 \text{ mm s}^{-1}$  and different isomer shifts  $\delta \approx 0.025$  and  $0.807 \text{ mm s}^{-1}$ . These parameters are typical of the  $\text{Fe}^{3+}$  and  $\text{Fe}^{2+}$  states, respectively. It can be suggested that the paramagnetic Mössbauer lines relate to the isocubanite phase  $\text{CuFe}_2\text{S}_3$ , which has both ferric and ferrous ions in tetrahedral sulfur sites and is nonmagnetic at room temperature. The crystal structure of isocubanite, which is a cubic polymorph of cubanite, is very similar to the chalcopyrite structure and both these phases may appear in the synthesis process. Isocubanite shows very strong lines in its XRD pattern which match well with the X-ray lines of chalcopyrite [47,48] and only Mössbauer parameters can distinguish between these phases. In our studies, we succeeded in synthesizing a pure phase of isocubanite nanoparticles by a method similar to the thermal pyrolysis route of chalcopyrite and these findings will be published elsewhere soon.

On the other hand, it is known that chalcopyrite  $\text{CuFeS}_2$  can exist in three phases:  $\alpha$ - $\text{CuFeS}_2$  is tetragonal with  $a = 5.25$  and  $c = 10.32 \text{ \AA}$ ;  $\beta$ - $\text{CuFeS}_2$  is cubic with  $a = 10.06 \text{ \AA}$ ; and  $\gamma$ - $\text{CuFeS}_2$  is tetragonal with  $a = 10.58$  and  $c = 5.37 \text{ \AA}$  [28,31,45]. The  $\alpha$ -phase is antiferromagnetic, the  $\beta$ -phase is ferromagnetic and the  $\gamma$ -phase is nonmagnetic down to 78 K [46,49]. It is possible that the nonmagnetic doublet components in our samples correspond to the  $\gamma$ -phase of chalcopyrite.

#### 4. Summary

A thermal pyrolysis route has been developed to synthesize the tetragonal phase of chalcopyrite  $\text{CuFeS}_2$  nanoparticles. The nanoparticles are single crystals and have a brick-like morphology. The “bricks” are self-organized

normal to the (1 1 2) crystal plane with the brick’s long axis in this plane, thus creating well-ordered anisotropic nanocomposites. HRTEM and electron diffraction data clearly show that every nanobrick is a single crystal with a layered atomic structure. The characteristic dimension of nanobricks is about  $5 \text{ nm} \times 20 \text{ nm}$  in plane. Magnetic measurements support the antiferromagnetic spin structure and reveal the appearance of a small ferromagnetic component below 60 K. This correlates with the anomalous behavior of the magnetic susceptibility found in bulk chalcopyrite, which was explained by the magnetic ordering of Cu atoms [12]. On the other hand, the low-temperature anomalies in susceptibility, magnetization and heat capacity were also explained by the existence of non-interacting ferromagnetic clusters appearing due to the disordering of Fe and Cu atoms in the chalcopyrite crystal lattice [36]. The maximum in the ZFC curves observed at low temperatures may be related to the superparamagnetic properties of the  $\text{CuFeS}_2$  nanoparticles. The Mössbauer spectra of the nanobricks show that only about 50% of the Fe atoms are in the magnetic  $\alpha$ -phase of chalcopyrite. The remaining Fe is nonmagnetic and may be located either in the  $\gamma$ -phase of chalcopyrite or in isocubanite. The presence of Fe in the intercalating compound separating the single-crystal nanobricks is also not excluded.

Recently, brick-like nanoparticles of chalcostibite  $\text{CuSbS}_2$  have been synthesized [50] using a hot-injection method with coordinating solvents. In contrast to our synthesis method, the  $\text{CuSbS}_2$  nanobricks were randomly oriented and do not form ordered composites. It was shown that the  $\text{CuSbS}_2$  nanobricks possess a band gap of 1.40 eV. About 5–15% of the visible light can be converted to electron and hole pairs in a photoelectrochemical cell using the  $\text{CuSbS}_2$  nanobrick-electrode, which demonstrates the potential application of such nanobricks in the field of solar energy conversion.

#### Acknowledgments

We thank Prof. A.S. Avilov for his help in the analysis of electron diffraction data. This work is supported by the Russian Foundation for Basic Research (Grant No. 11-02-92001) and the Russian Academy of Sciences under the Program “Nanotechnology and Nanomaterials” (Grant No. 21-4.1.7). We also thank the National Science Council of Taiwan (NSC100-2923-M-218-001-MY3) for financial support.

#### References

- [1] Disalvo FJ. Science 1991;247:649.
- [2] Alivisatos AP. Science 1996;271:933.
- [3] Heath JR, Kuekes PJ, Synder G, Williams RS. Science 1998;280:1717.
- [4] Fuertes Marron D, Canovas E, Levy MY, Marti A, Luque A, Afshar M, et al. Sol Energy Mater Sol Cells 2010;94:1912.
- [5] Fuertes Marron D, Marti A, Luque A. Phys Status Solidi A 2009;206:1021.
- [6] Marti A, Fuertes Marron D, Luque A. J Appl Phys 2008;103:073706.

- [7] Yue GH, Yan PX, Liu JZ, Wang MX, Li M, Yuan XM. *J Appl Phys* 2005;98:103506.
- [8] Yue GH, Yan PX, Fan XY, Wang MX, Qu DM, Wu ZG, et al. *Electrochem Solid-State Lett* 2007;10:D29.
- [9] Broido DA, Reinecke TL. *Appl Phys Lett* 1995;67:100.
- [10] Yue GH, Yan PX, Fan XY, Wang MX, Qu DM, Yan D, et al. *J Appl Phys* 2006;100:124313.
- [11] Ivanov VA, Aminov TG, Novotortsev VM, Kalinnikov VT. *Russ Chem Bull Int Ed* 2004;11:2255 [Izv. Akad. Nauk, Ser. Khim. 2004;11:2255].
- [12] Khabibullin IK, Garif'yanov NN, Matukhin VL. *Russ Phy J* 2008;51:767.
- [13] Shay JL, Wernick LH. Ternary chalcopyrite semiconductor: growth electronic properties and applications. Oxford: Pergamon Press; 1975.
- [14] Shafarman WN, Stolt L. In: Luque A, Hegedus S, editors. *Handbook of photovoltaic science and engineering*. Chichester: Wiley; 2002. p. 567.
- [15] Jihun Oh, Yuan Hao-Chih, Branz Howard M. *Nat Nanotechnol* 2012;7:743–8. <http://dx.doi.org/10.1038/nnano.2012.166>.
- [16] Barkat L, Hamdadou N, Morsli M, Khelil A, Bernede JC. *J Cryst Growth* 2006;297:426.
- [17] Wang MX, Wang LS, Yue GH, Wang X, Yanc PX, Peng DL. *Mater Chem Phys* 2009;115:147.
- [18] Disale Sujit D, Garje Shivram S. *Appl Organometal Chem* 2009;23:492–7.
- [19] Wang Chunrui, Xue Shaolin, Junqing Hu, Tang Kaibin. *Jpn J Appl Phys* 2009;48:023003.
- [20] Wang Yu-Hsiang A, Bao Ningzhong, Gupta Arunava. *Solid State Sci* 2010;12:387–90.
- [21] Liang Daxin, Ma Ruoshui, Jiao Shihui, Feng Guangsheng Pangand Shouhua. *Nanoscale* 2012;4:6265–8.
- [22] Panda SK, Datta A, Dev A, Gorai S, Chaudhuri S. *Cryst Growth Des* 2006;6:2177.
- [23] Duan X, Huang Y, Agarwal R, Lieber CM. *Nature* 2003;421:241.
- [24] Yue GH, Yan PX, Wang LS, Wang W, Chen YZ, Peng DL. *Nanotechnology* 2008;19:195706.
- [25] Gurin VS. *Colloids Surf A* 1998;142:35–40.
- [26] Kradinova LV, Polubotko AM, Popov VV, Prochukhan VD, Rud Yu V, Skorukin VE. *Semicond Sci Technol* 1993;8:1616.
- [27] Teranishi VT. *J Phys Soc Jpn* 1961;16:1881.
- [28] Donnay G, Corliss L, Donnay JDH, Elliot N, Hastings JM. *Phys Rev* 1958;112:1917.
- [29] Hamajima T, Kambara T, Gondaira KI, Oguchi T. *Phys Rev B* 1981;24:3349.
- [30] Hu JQ, Lu QY, Deng B, Tang KB, Qian YT, Zhou GE, et al. *Inorg Chem Commun* 1999;2:569.
- [31] Pauling L, Brockway LO. *Z Krist* 1932;82:188.
- [32] Pearce CI, Pattrick RAD, Vaughan DJ, Henderson CMB, Van der Laan G. *Geochim Cosmochim Acta* 2006;70:4635.
- [33] Langford JI, Wilson AJC. *J Appl Cryst* 1978;11:102.
- [34] Jackson AM, Myerson JW, Stellacci F. *Nat Mater* 2004;3:330.
- [35] Lotgering FK. In: *Proc int conf magnetism, Nottingham; 1964*. p. 533.
- [36] Popov VV, Kizaev SA. *Rud' Yu V Fiz Tverd Tela* 2011;53:70.
- [37] Hu J, Lu Q, Deng B, Tang K, Qian Y, Li Y, et al. *Inorg Chem Commun* 1999;2:569.
- [38] Vaughan DJ, Tossell JA. *Science* 1973;179:375.
- [39] Ok HN, Back KS, Choi EJ. *Phys Rev B* 1994;50:10327.
- [40] Diguseppe M, Steger J, Wold A, Kostiner E. *Inorg Chem* 1974;13:1828.
- [41] Ok HN, Kim CS. *Nuovo Cimento* 1975;28B:138.
- [42] Boekema C, Krupski AM, Varasteh M, Parvin K, van Til F, van der Wonde F, et al. *J Magn Magn Mater* 2004;272–276:559.
- [43] Walker LR, Wertheim GK, Jaccarino V. *Phys Rev Lett* 1961;6:98.
- [44] Vaughan DJ, Craig JR. In: Harland WB, Agrell SO, Cook AH, Hughes NF, editors. *Mineral chemistry of metal sulfides*. Cambridge: Cambridge University Press; 1978. p. 154.
- [45] Hiller JE, Probsthain K. *Z Krist* 1956;108:108.
- [46] Adams R, Beaulien R, Vassiladis M, Wold A. *Mater Res Bull* 1972;7:87.
- [47] Caye R, Cerverle B, Cesbron F, Oudin E, Picot P, Pillard F. *Mineral Mag* 1988;52:509.
- [48] Pareek S, Rais A, Tripathi A, Chandra U. *Hyperfine Interact* 2008;186:113.
- [49] Eissa NA, Sallam HA, El-Ockr MM, Mahmoud EA, Saleh SA. *J de Physique, Colloque* 1976;C6(Suppl. v37#12):C6–793.
- [50] Yan Chang, Zhenghua Su, Ening Gu, Cao Tiantian, Yang Jia, et al. *Roy Soc Chem: RSC Adv* 2012;2:10481–4.